Chalmers Publication Library

Phase coherence and energy relaxation in epitaxial graphene under microwave radiation

(article starts on next page)

Phase coherence and energy relaxation in epitaxial graphene under microwave radiation

V. Eless, T. Yager, S. Spasov, S. Lara-Avila, R. Yakimova, S. Kubatkin, T. J. B. M. Janssen, A. Tzalenchuk, and V. Antonov
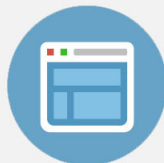
Phase coherence and energy relaxation in epitaxial graphene under microwave radiation

V. Eless,[1,2,a)] T. Yager,[3] S. Spasov,[2] S. Lara-Avila,[3] R. Yakimova,[4,5] S. Kubatkin,[3] T. J. B. M. Janssen,[1] A. Tzalenchuk,[1,2] and V. Antonov[2]

[1]*National Physical Laboratory, Hampton Road, Teddington TW11 0LW, United Kingdom*
[2]*Physics Department, Royal Holloway, University of London, Egham, Surrey TW20 0EX, United Kingdom*
[3]*Department of Microtechnology and Nanoscience (MC2), Chalmers University of Technology, S-41296 Göteborg, Sweden*
[4]*Department of Physics, Chemistry and Biology (IFM), Linköping University, S-58183 Linköping, Sweden*
[5]*Graphensic AB, S-58330 Linköping, Sweden*

We have performed low-temperature magnetotransport measurements on monolayer epitaxial graphene under microwave radiation and extracted the radiation-induced effective temperatures, energy relaxation, and the dephasing times. We established that the response of the graphene sample is entirely bolometric at least up to 170 GHz. Dynamic dephasing, i.e., the time-reversal symmetry breaking effect of the ac electromagnetic field rather than mediated by heating, may become significant in the terahertz frequency range and in samples with longer phase coherence time. [http://dx.doi.org/10.1063/1.4819726]

Carrier energy loss rates determine how the electrons cool down when heated above the lattice temperature. They influence thermal dissipation and heat management in graphene electronics[1–3] as well as low-temperature applications such as quantum resistance metrology[4,5] and hot-electron bolometers.[6,7] Energy loss rates have previously been measured in exfoliated, CVD and epitaxial graphene grown on SiC using dc current heating of the electrons above the lattice temperature.[8–11] At the same time, many of the proposed applications of graphene both at room- and at low temperatures involve operation at high frequencies.[12,13] To evaluate the low-temperature performance of epitaxial graphene exposed to microwave radiation, we used quantum corrections to conductivity to find the electron temperature and determine the loss rates.

Quantum corrections to the charge transport in graphene have been extensively studied over the recent years.[14–17] The corrections arise from the localization and interaction effects in the disordered Fermi liquid. The weak localisation (WL) correction to the conductivity is due to the coherence of electrons traversing the same trajectories in opposite directions. Experimentally, it manifests itself in negative magnetoresistance around the zero magnetic field. Any violation of the symmetry with respect to time reversal leads to dephasing. The symmetry breaking processes include all inelastic processes, e.g., scattering on electrons, phonons, or localised spins, dephasing due to static magnetic field or alternating electromagnetic field. The latter effect was studied theoretically[18] and to some extent experimentally[19,20] in conventional 2DEGs, but not until now in graphene.

Interaction of microwave radiation with the electrons can, in principle, lead to two distinct effects, each contributing to the change in conductivity.

The absorption of radiation by the electron system leads to its heating to a temperature T_e above the lattice temperature

T_L, governed by the energy relaxation time τ_e. The increase in T_e leads to the suppression of τ_ϕ and consequently alters the WL correction to conductivity. In addition, the in-plane high-frequency electric field modifies the WL contribution to conductivity directly. Both the direct and indirect (through heating) effect of microwaves on WL increase with microwave power. Any direct suppression of quantum coherence in graphene due to microwave radiation (dynamic dephasing) has to be distinguished from a contribution from the heating effect of the electromagnetic field. Therefore, temperature dependence of WL correction to conductivity cannot *a priori* be used for the electron thermometry under high-frequency excitation. WL and electron-electron (EE) interaction corrections to the conductivity depend on the temperature in the same way, but they can be separated by suppressing WL in magnetic field. At low temperatures and once WL is suppressed, the conductivity only depends on temperature through the EE interaction, which can be used as an electron thermometer.

The investigated graphene samples were grown on the Si-terminated face of silicon carbide (SiC (0001)) by graphitisation at 2000 °C in 1 atm of argon. They are *n*-doped with carrier concentration and mobility of $n \approx 5 \times 10^{11}$ cm^{-2} and $\mu \approx 7.5 \times 10^3$ cm^2/V s at 4 K correspondingly. Nine devices were fabricated on a 7×7 mm^2 chip. Two devices had a Hall bar geometry with eight electrical contacts, which allowed for four-terminal measurements of the longitudinal and Hall resistance. These devices were used in microwave measurements up to 10 GHz. Further nine devices were used in measurements at 170 GHz and will be described later in the text. All devices showed similar behaviour with a parameter variation of $\approx 10\%$. The whole chip was covered with a polymer bilayer (PMMA-MAA/ZEP520A) both for protection of graphene devices and to enable photochemical control of the charge carrier density in graphene by deep UV light.[21]

In a magnetic field, sufficient to completely suppress weak localisation, the influence of alternating electromagnetic fields on the conductivity reduces simply to the heating of the

a)vbe@npl.co.uk

electron system and the residual temperature dependence is due to the EE interactions. In this regime, therefore we can relate the effective temperature of the electrons to the power of the alternating electromagnetic field by comparing the change in conductance (or resistance) due to power and due to the ambient temperature. Theoretically, WL is completely suppressed in the field 0.3–0.4 T at which the magnetic length ($l_B = \sqrt{\hbar/2eB}$) becomes comparable to the mean free path in our samples ($l \approx 45$–50 nm). Experimentally, however, we found that the resistance is flat between 0.1 and 0.6 T and all analysis has been performed in the range $B \leq |0.2|$ T. Figure 1 illustrates the power-to-temperature calibration procedure for one representative set of data.

To quantify the influence of microwave radiation on quantum coherence, we plot the inverse phase coherence time τ_ϕ^{-1} as a function of the (effective) temperature (Figure 2). The phase coherence time was determined by fitting the weak localisation peak to the theory.[22] The zero field, temperature-dependent analytic correction due to localization effects in graphene reads

$$\Delta\rho_{WL-Fit}(B=0,\bar{T}) = \frac{e^2\rho^2}{\pi h}\left[\ln\left(1+2\frac{\tau_\phi}{\tau_i}\right) - 2\ln\left(\frac{\tau_\phi/\tau_{tr}}{1+\tau_i/\tau_*}\right)\right],$$

(1)

where the relaxation time is calculated as $\tau_{tr} = l/v_F = h/(2e^2\rho_{xx}v_F\sqrt{\pi n}) \approx 0.05$ ps and the scattering times τ_ϕ, τ_i (intervalley), τ_* (intravalley) are found by fitting the measured $\rho_{xx}(B,\bar{T})$ to Eq. (2)

$$\frac{\Delta\rho(B,\bar{T})}{\rho^2} = -\frac{e^2}{\pi h}\left[F\left(\frac{B}{B_\phi}\right) - F\left(\frac{B}{B_\phi+2B_i}\right) - 2F\left(\frac{B}{B_\phi+B_*}\right)\right]$$

(2)

with $F(z) = \ln(z) + \Psi(\frac{1}{2}+\frac{1}{z})$ and $\tau_{\phi,i,*} = \frac{\hbar}{4De}B_{\phi,i,*}^{-1}$.

The conclusion from Figure 2 is that the microwave radiation has exactly the same effect on quantum coherence as the change in the electron temperature. This means that the response is entirely bolometric in the whole parameter space studied and that the dynamic dephasing process is negligible.

FIG. 2. Inverse phase coherence time and, inset, length as a function of the effective temperature.

The fastest scattering process determining the electron momentum relaxation rate is scattering on donors on the SiC surface, whereas τ_i and τ_* are much longer. We also note that the fits are not particularly sensitive to the values of τ_i and τ_*, but qualitatively we conclude that they are virtually temperature-independent.

The values of the phase coherence length $L_\phi = \sqrt{D\tau_\phi}$, resulting from the fit to the WL theory are presented in Figure 2 inset. At low temperatures, L_ϕ reaches the micrometer range. The dashed line shows the fit to $T^{-1/2}$ in the appropriate temperature range.

The energy relaxation rate per carrier P is determined as $P = \frac{W}{nA}$, where W is the heating power, n—carrier density and A—area of the sample. The relaxation rate depends on the temperature of the electrons resulting from the heat, T_e and the temperature of the lattice T_L. Above we have established the effective electron temperature of a graphene sample upon microwave excitation. Figure 3 shows the scaling of the temperature with microwave power, $W_{\mu w}$. The same heating effect is produced by dc power dissipation W_{dc}. In both cases, the power is $\propto (T_e^3 - T_L^3)$ in agreement with our conclusion that microwave excitation of a graphene sample results only in heating. This scaling is consistent with the supercollision cooling mechanism[23] and was previously observed at relatively high T_L in experiments using dc current heating[11,24] and optical excitation.[25] Comparing the
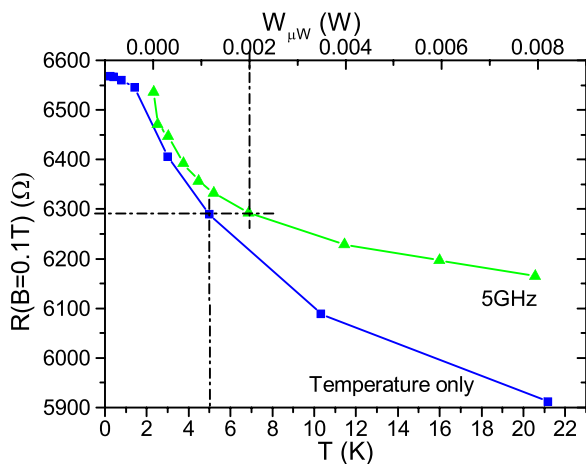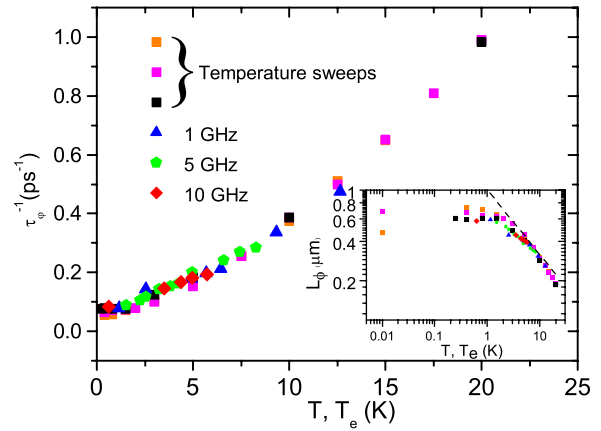

FIG. 1. Comparison between the effect of ambient temperature and microwave radiation on the sample resistance in a magnetic field suppressing WL. Dashed lines illustrate the $W_{\mu w}$-to-T_e calibration.
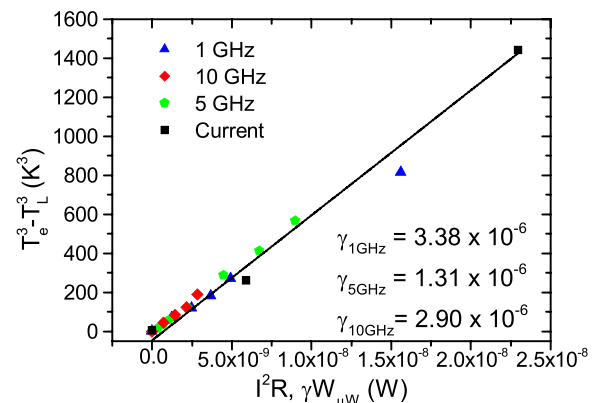

FIG. 3. Scaling of the electron temperature with the dissipated dc electric power and the microwave power at various frequencies.

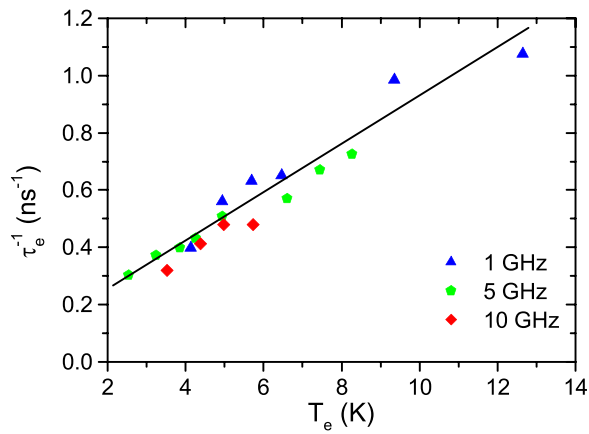FIG. 4. Inverse energy relaxation time as a function of the effective temperature.

FIG. 6. Response of a graphene device in Figure 5(a) to 170 GHz radiation.

slopes, we determine both the frequency-dependent coupling coefficient γ of the microwave power $W_{\mu w}$ to the sample and the energy relaxation rate. From $W_{dc} = I^2 R = \alpha(T_e^3 - T_L^3)$, we get $\alpha = 5.38 \times 10^{-18}\,\mathrm{W\,K^{-3}}$. Equating $W_{dc} = \gamma W_{\mu w} = \alpha(T_e^3 - T_L^3)$, we get γ in the range of 10^{-6} slightly varying for different frequencies.

Further, we determine the energy relaxation time as $\tau_e = \frac{\pi^2 k_b^2 T_e^2}{3 E_F P} = \frac{\pi^2 k_b^2 T_e^2}{3 E_F \alpha(T_e^3 - T_L^3)}$ for different frequencies and microwave powers, Figure 4. As expected for high electron overheating against the lattice, $T_e \gg T_L$, $\tau_e \propto 1/T_e$.

Using frequencies of 1 to 10 GHz, we have found $\tau_e > 1$ ns. From Figure 2, we obtain τ_ϕ in the range 1–15 ps. Thus for all microwave powers, we find that $\tau_e \gg \tau_\phi$. We can now compare the experimentally established characteristic times with the period of microwave radiation t. $t = 2\pi/f$ is in the range between 0.6 and 7 ns and therefore $\tau_\phi \ll t \approx \tau_e$. So, while there is enough time to establish the temperature in the electron system over the period of microwave radiation, there is not enough time to induce the dynamic dephasing. The latter process may become significant at frequencies in the terahertz range.

To probe the response of the graphene sample to electromagnetic radiation at much higher frequencies, we used a quasioptical scheme shown in Figure 5. The graphene sample was fitted with a log-periodic antenna to enhance coupling (Fig. 5(a)). The sample thermalised at the cold stage of an optical cryostat was illuminated by a Gunn diode emitting at 170 GHz through a series of filtered windows installed at
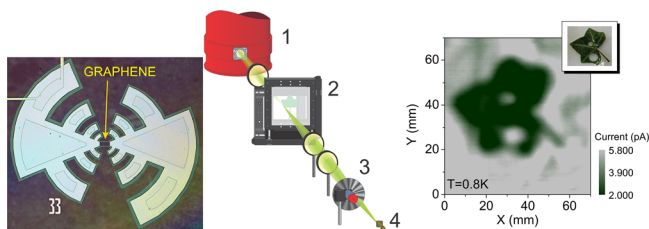
different stages inside the cryostat (Fig. 5(b)). A graphic illustration of the sample response to the incident radiation is shown in Fig. 5(c): an ivy leaf was raster-scanned under the beam and the sample response was recorded as a function of the leaf position. The leaf attenuates the radiation power incident on the graphene sample.

In Figure 6, we show that the sample response to even 170 GHz radiation is entirely bolometric. As before we determined the radiation-induced effective electron temperature by suppressing the weak localisation peak in magnetic field and comparing the conductance change associated with the sub-terahertz radiation with that due to change in the ambient temperature. We then adopted a simplified analytical approach, whereby we compare the change in the amplitude of the weak localisation peak at any given radiation-induced effective electron temperature and the corresponding ambient temperature, rather than the full τ_ϕ analysis. Both approaches give similar results. We see that the amplitude of the weak localisation correction to conductivity is again entirely determined by the temperature of the electrons.

In summary, we have shown that the response to microwave radiation of an epitaxial graphene sample produced on SiC (0001) is entirely bolometric, i.e., due to heating of the electron gas, up to at least 170 GHz and established the energy relaxation and the phase coherence times from microwave measurements.

Direct dephasing process may become important at THz frequencies and in graphene samples with longer phase coherence. In monolayer graphene on SiC (0001) τ_ϕ is limited by spin-flip scattering at low temperatures. The spin-flip process can be suppressed by in-plane magnetic field.[26,27] Alternatively, for observation of the dynamic dephasing, one can use multilayer graphene on SiC (000$\bar{1}$).

FIG. 5. (a) Optical micrograph of a $100 \times 60\,\mu\mathrm{m}^2$ graphene strip placed in the centre of a log-periodic antennae; (b) Measurement setup: (1) refrigerator with the graphene sensor, (2) XY translation stage, (3) mechanical chopper, (4) Gunn diode source; (c) False-colour image of an ivy leaf illuminated by 170 GHz radiation from the Gunn diode and detected by a voltage biased (1 mV) graphene device held at T = 0.8 K; Inset: optical image of the same leaf.

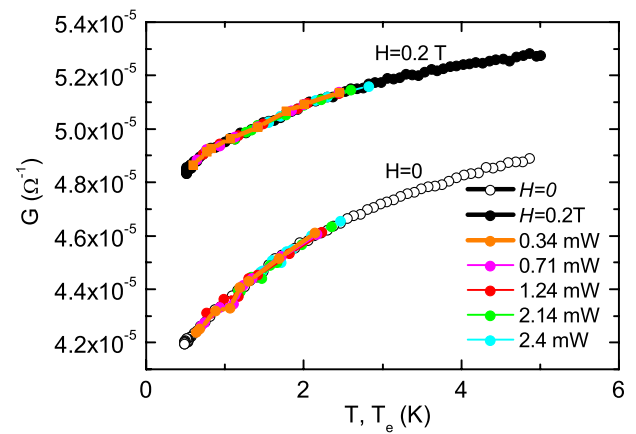[1]A. A. Balandin, Nature Mater. **10**, 569–581 (2011).
[2]K. M. Shahil and A. A. Balandin, Solid State Commun. **152**, 1331–1340 (2012).

3D. L. Nika and A. A. Balandin, J. Phys.: Condens. Matter **24**, 233203 (2012).

4A. Tzalenchuk, S. Lara-Avila, A. Kalaboukhov, S. Paolillo, M. Syvajarvi, R. Yakimova, O. Kazakova, T. J. B. M. Janssen, V. Fal'ko, and S. Kubatkin, Nat. Nanotechnol. **5**, 186–189 (2010).

5T. J. B. M. Janssen, N. E. Fletcher, R. Goebel, J. M. Williams, A. Tzalenchuk, R. Yakimova, S. Kubatkin, S. Lara-Avila, and V. I. Falko, New J. Phys. **13**, 093026 (2011).

6J. Yan, M. H. Kim, J. A. Elle, A. B. Sushkov, G. S. Jenkins, H. M. Milchberg, M. S. Fuhrer, and H. D. Drew, Nat. Nanotechnol. **7**, 472–478 (2012).

7K. C. Fong and K. C. Schwab, Phys. Rev. X **2**, 031006 (2012).

8Z. Tan, C. Tan, L. Ma, G. T. Liu, L. Lu, and C. L. Yang, Phys. Rev. B **84**, 115429 (2011).

9A. C. Betz, F. Vialla, D. Brunel, C. Voisin, M. Picher, A. Cavanna, A. Madouri, G. Fève, J. M. Berroir, B. Plaçais, and E. Pallecchi, Phys. Rev. Lett. **109**, 056805 (2012).

10A. M. R. Baker, J. A. Alexander-Webber, T. Altebaeumer, and R. J. Nicholas, Phys. Rev. B **85**, 115403 (2012).

11A. M. R. Baker, J. A. Alexander-Webber, T. Altebaeumer, S. D. McMullan, T. J. B. M. Janssen, A. Tzalenchuk, S. Lara-Avila, S. Kubatkin, R. Yakimova, C. T. Lin, L. J. Li, and R. J. Nicholas, Phys. Rev. B **87**, 045414 (2013).

12Y.-M. Lin, C. Dimitrakopoulos, K. A. Jenkins, D. B. Farmer, H.-Y. Chiu, A. Grill, and P. Avouris, Science **327**, 662 (2010).

13Y.-M. Lin, A. Valdes-Garcia, S.-J. Han, D. B. Farmer, I. Meric, Y. Sun, Y. Wu, C. Dimitrakopoulos, A. Grill, P. Avouris, and K. A. Jenkins, Science **332**, 1294–1297 (2011).

14F. V. Tikhonenko, D. W. Horsell, R. V. Gorbachev, and A. K. Savchenko, Phys. Rev. Lett. **100**, 056802 (2008).

15F. V. Tikhonenko, A. A. Kozikov, A. K. Savchenko, and R. V. Gorbachev, Phys. Rev. Lett. **103**, 226801 (2009).

16S. Lara-Avila, A. Tzalenchuk, S. Kubatkin, R. Yakimova, T. J. B. M. Janssen, K. Cedergren, T. Bergsten, and V. Fal'ko, Phys. Rev. Lett. **107**, 166602 (2011).

17J. Jobst, D. Waldmann, I. V. Gornyi, A. D. Mirlin, and H. B. Weber, Phys. Rev. Lett. **108**, 106601 (2012).

18V. I. Fal'ko, Sov. Phys. JETP **65**, 397–399 (1987).

19S. A. Vitkalov, G. M. Gusev, Z. D. Kvon, and G. I. Leviev, JETP Lett. **43**, 185–188 (1986).

20S. A. Vitkalov, G. M. Gusev, Z. D. Kvon, G. I. Leviev, and V. I. Fal'ko, Sov. Phys. JETP **67**, 1080–1084 (1988).

21S. Lara-Avila, K. Moth-Poulsen, R. Yakimova, T. Bjornholm, V. Fal'ko, A. Tzalenchuk, and S. Kubatkin, Adv. Mater. **23**, 878 (2011).

22E. McCann, K. Kechedzhi, V. I. Fal'ko, H. Suzuura, T. Ando, and B. L. Altshuler, Phys. Rev. Lett. **97**, 146805 (2006).

23J. C. W. Song, M. Y. Reizer, and L. S. Levitov, Phys. Rev. Lett. **109**, 106602 (2012).

24A. C. Betz, S. H. Jhang, E. Pallecchi, R. Ferreira, G. Feve, J. M. Berroir, and B. Placais, Nat. Phys. **9**, 109–112 (2013).

25M. W. Graham, S.-F. Shi, D. C. Ralph, J. Park, and P. L. McEuen, Nat. Phys. **9**, 103–108 (2013).

26E. McCann and V. I. Fal'ko, Phys. Rev. Lett. **108**, 166606 (2012).

27M. B. Lundeberg, R. Yang, J. Renard, and J. A. Folk, Phys. Rev. Lett. **110**, 156601 (2013).